Actuating and Energy Absorbing Textiles Composed of NiTi Microfilament Over-twisted Coiled Yarns

Charles A. Weinberg*[a], Song Cai[b], Jeremy E. Schaffer[b], Julianna M. Abel[a]
[a]Department of Mechanical Engineering, University of Minnesota, Minneapolis, MN, USA 55455;
[b]Fort Wayne Metals, 9609 Ardmore Ave., Fort Wayne, IN, USA 46809

ABSTRACT

Traditional textile structures made of multifunctional materials leverage unique material behaviors through a hierarchical manufacturing process to develop tailored solutions applicable to robotic, transportation, and medical device industries. For example, knitted and woven textiles made of shape memory materials can provide high force and distributed motions for programmable surfaces, soft robotic grippers, and active compression garments. Additionally, 3D spacer fabrics with superelastic materials can provide constant force profiles, enhanced damping frequency ranges, and large energy dissipations for prosthetic attachments, helmet technology, and impact resistance fortifications. Usually, researchers manufacture multifunctional textiles with monofilament and yarns but recently, over-twisted coiled structures have demonstrated improved actuation contractions, force generations, and strain recovery. This research presents the creation of NiTi microfilament over-coiled yarns within textile structures, demonstrating their dual potential as high force linear actuators from the shape memory effect, and compact energy absorbers from superelasticity. To highlight the actuation potential of NiTi over-twisted coiled yarn textiles, the coiled yarns were integrated in parallel within a woven textile. The over-twisted coiled weave was experimentally investigated for actuation contractions, and generated forces. For energy absorption, the NiTi over-twisted coiled yarns were structured within a 3D spacer textile structure, and experimentally investigated quasi-statically for strain recovery and energy absorption through hysteresis, as well as dynamically for mapping damping performance dependent behavior. This work expands the profile of NiTi based multifunctional textiles to offer improved and tailored solutions for actuating and energy absorbing technologies.

Keywords: Shape Memory Alloys, Coiled Yarns, Multifunctional Textiles, Energy Absorption, Actuation, Damping, Medical Compression

1. INTRODUCTION

Traditional actuating systems such as pneumatics, hydraulics, and electromagnetics are usually heavy, bulky, and are specifically applied to narrow applications. For this reason, researchers are pushing to create compact, soft, and compliant artificial muscles and energy absorbers for robotic, medical device, and defense applications [1]-[13]. Artificial muscles are achieved from a broad range of solutions ranging from multifunctional material systems such as dielectric elastomers, piezoelectrics, shape memory materials, and liquid crystal elastomers, to geometric and structural leveraging such fiber reinforced and pleated pneumatic structures [14]. Recently, researchers have leveraged the unique properties from multifunctional material systems in novel 1D form factors such as twisted yarns, mandrel wrapped coils, and over twisted coils to enhance actuation capabilities. Of these, coiled yarns have shown great promise because of their inherent compactness, flexibility, high power to weight ratio, potential for scalability, and easy use with a wide range of materials [15]-[21]. However, as a standalone coil structure, parameters are limited to bundle configurations (number of filaments, filament diameter) and thermal processing conditions. Because of the inherent hierarchical manufacturing approach, textiles provide designers more tunable parameters to match structural performance to desirable application needs. Functionalized integrated coiled yarn textiles provide the means for designers to achieve desirable performance by tuning textile structure, textile density, and number of coils in addition to coiled yarn parameters.

One material system that has significant potential in coiled yarns, but has yet to be explored, are shape memory alloys (SMA). Shape memory alloys (SMA), such as nickel-titanium (NiTi), leverage a solid-state phase transformation to produce large actuation forces [22]-[23]. The solid-state phase transformation occurs when the material is heated above its characteristic austenite finish temperature (A_F), which can be tailored through chemical composition modifications, heat treatment, and cold working [24]-[28]. The transformation from martensite to austenite, enables the recovery of elastic and plastic strains through the change of lattice structures, which ultimately causes the shape memory effect [22]. A similar

solid phase transformation occurs without thermal activation when loading is applied at temperatures above A_F, called superelasticity. Strains associated with a stressed induced martensitic phase are hysteretically recovered through the passive transformation back to austenite upon unloading. [29]. Leveraging the shape memory effect and superelasticity in a coiled yarn could provide high force actuations and large strain recoveries in a 1D structure capable of being integrated in multifunctional textiles.

This paper presents the creation of NiTi microfilament over-twisted coiled yarns within textile structures as actuators for soft robotic, and medical device applications such as medical compression garments, as well as energy absorbers for defense, impact, and damping applications. Over-twisted coiled yarn structures are created on a custom-built manufacturing system by inserting twist into a bundle of NiTi microfilaments until the torsional imbalance imparted on the yarn causes coils in the direction of the yarn axis to form. The coiled yarns are thermally processed to shift transformation temperatures and shape set the final coiled structure. Superelastic and actuating performance are investigated demonstrating high force actuations and extended strain recoveries. To exhibit their functionality in a textile structure, a 2D woven textile was manufactured on small hobbyist loom by placing the coiled yarns vertically in parallel and interweaving a Kevlar yarn perpendicularly to the coiled yarns. The woven textile provides increased actuated forces, a low force martensitic response, and increased optimization capabilities. To demonstrate the superelastic and energy absorbing potential, a second textile in the form of a 3D spacer fabric was manufactured. 3D spacer fabrics consist of two outer knitted layers connected and distanced by a spacer yarn, which gives the fabric it's 3D form. The 3D spacer fabric leverages both traditional structural effects as well as the unique energy absorbing behaviors of superelastic NiTi. The NiTi coiled yarn spacer fabric exhibited potential as a high force energy absorber and future optimizations are discussed to improve performance. NiTi coiled yarns are novel 1D structures enabling new multifunctional textiles for scalable actuations and high force energy absorption for medical device, defense, and transportation industries.

2. MATERIALS & MANUFACTURING

2.1 Materials

The manufacturing of NiTi over-twisted coiled yarns was permitted by the creation of NiTi filaments with diameters in the micron-range. A bundle of NiTi microfilaments are dictated by the number of filaments and diameter of the individual filaments. For this work, bundles containing 800 filaments with diameters of 10µm were used (800-10). The NiTi alloy used in this study has a chemical composition of 56 wt. % nickel with 300ppm oxygen, 310ppm carbon, and balanced titanium. It is a nickel-rich material, with an ingot A_f of 68°C. Digital scanning calorimetry (DSC) of pre-thermally processed microfilament bundles exhibited unstable transformations (multiple austenitic transformation peaks and broad transformation ranges of 24°C) and extreme transformation temperatures (martensite start temperature, M_S=-53.9°C; martensite finish temperature, M_F=undefined). After coiled yarn manufacturing, the structures were fixed in place and thermally processed to stabilize transformations and increase the martensite finish temperature. Over-twisted coiled yarns were heated in air at 550°C for 11 minutes as determined by a design of experiments. Post-thermally processed microfilament bundles demonstrated stabilized transformation temperatures (austenite finish, A_F=52.2ºC; austenite start, A_S=40.7; martensite start, M_S=-10.3ºC, martensite finish M_F=-22.7ºC) that were compatible with the temperature ranges of the environmental chamber for mechanical characterization.

2.2 Over-twisted coiled yarn manufacturing

A custom-built coil manufacturing rig inserts twist into a microfilament bundle at an applied tension load to manufacture over twisted coiled yarns (Figure 1a). When a bundle of filaments is twisted, a torsional imbalance is created in the yarn resulting in spontaneous coil forming in two directions. At low or zero tension, the yarn reconfigures in a torque balanced snarl (or pigtail) in a direction normal to the yarn axis (Figure 1b). As you increase the tension, axial homochiral cylindrical coil will form in multiple locations, however this can lead to defects in the coiled yarn (double coiling, uncoiled sections), that compromise the mechanical integrity of the structure (Figure 1b). At ideal tension, the yarn will form an axial homochiral cylindrical coil at a single location and propagate from there. At high tension, the yarn will break before any snarling occurs. To manufacture the coiled yarns, one end of a strand of a microfilament bundle is clamped directly into a

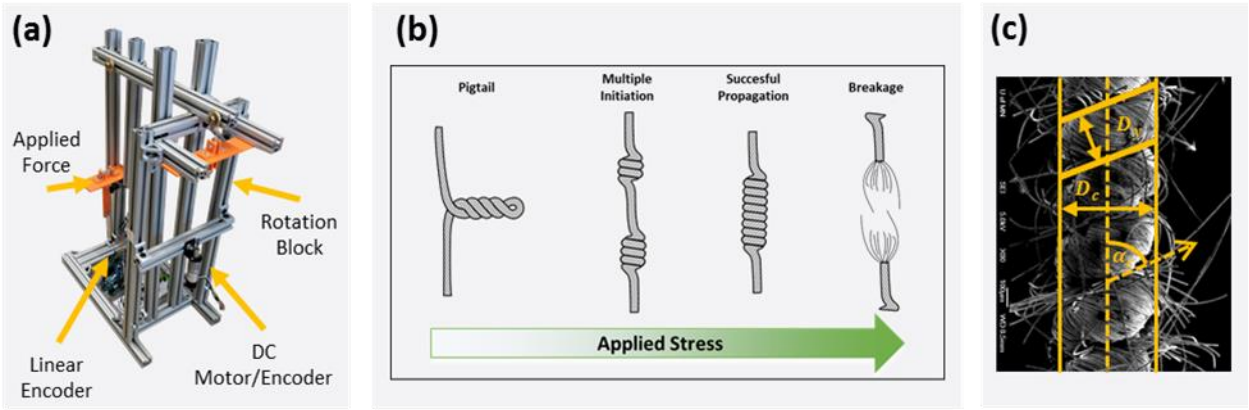

Figure 1. (a) Custom built coiled yarn manufacturing system capable of inserting twist in a rotationally constrained bundle of NiTi microfilaments. The system has the capability of tracking twist insertion as well as linear retraction during manufacturing. (b) The resultant structures formed from manufacturing at increasing applied stresses. At too light of stress, the yarn will pigtail perpendicularly to the yarn axis. Coil propagation exists in an ideal stress range, but ideally initiates from a single site and grows outward towards the ends. At too high of stress, the yarn will break instead of coiling in any direction. (c) SEM imaging of a NiTi coiled yarn for geometric characterization of the coiled yarn diameter (D_c), yarn diameter (D_y), and coil angle (α_c),

DC motor shaft, while the other is fixed on a custom 3D printed platform that restricts any further twisting, causing all inserted twist to act on the microfilament strand (Figure 1a). The custom 3D platform is connected by a pulley system to an applied weight to control the tension in the strand. During manufacturing, tracking of the inserted twist and strand length is done by a rotary encoder on the DC motor and a linear encoder strip attached along the pulley system. Thermal processing is required to shape set the NiTi filaments and remove the residual torsional stresses that remain in the coiled yarn structure after manufacturing. The coiled yarn is fixed in place after manufacturing and heat treated in a Lindberg/Blue M™ box furnace at 550°C for 11 minutes. As well as torsional stability, post-thermally processed coiled yarns demonstrated stabilized transformations that were compatible with the temperature ranges of the environmental chamber for mechanical characterization. After manufacturing, the over-twisted coiled yarns configurations were geometrically characterized in a scanning electron microscope (SEM) to identify the coil diameter (D_c), coil angle (α_c), and yarn diameter (D_y) (Figure 1c). The coil diameter is defined as the radial length of the global coil structure, while the yarn diameter is defined as the radial length of the yarn constituting a single coil. The coil angle describes the acute angle between the coil axis and yarn axis. On average, the 800-10 coiled yarns had coil diameters (D_c) of 0.8 mm, coil angles of 77°, and yarn diameters of 0.4 mm. The coil diameter corresponded to a coil area of 0.50 mm^2 which is used in normalized force calculations.

2.3 Coiled Yarn Textile Manufacturing

The manufacturing system was used to manufacture eight coiled yarns consisting of 800 filaments with 10µm diameters and a length of ~23cm for a woven textile. The eight coiled yarns were fixed in parallel under a light tension (50g) in a hobbyist loom in the warp (y) direction (Figure 2a). The hobbyist loom had warp slots spaced 8.5 mm apart. A Kevlar yarn was woven through the coiled yarns in the perpendicular weft (x) direction to hold the coiled yarns together (Figure 2b). To isolate the performance of the NiTi coiled yarns within the weave, Kevlar was chosen as the weft material because it has a small thermal expansion coefficient. The warp coiled yarns were cut to the same length and the final woven measured 57 x 160 mm in a stress-free austenitic state.

The weft knit energy absorbing spacer fabric was manufactured on a manually driven weft knitting machine Taitexma TH-260 with a fixed distance of 9mm between the knitting needles (Figure 2c) and a fixed distance of 12mm between knitting beds. The top and bottom fabric surfaces were knit with Kevlar yarn in a stockinette (jersey) pattern on two needle beds (Figure 2d). The spacer yarn consisted of the over-twisted NiTi coiled yarns and was wrapped in a crossing pattern in the x-z plane joining the two stockinette surfaces (Figure 2c). The thickness of the spacer fabric was dictated mainly by the spacing between the two needle beds. The final dimensions of the spacer fabric measured 40 x 30 x 10.5 mm in a stress-free austenitic state.

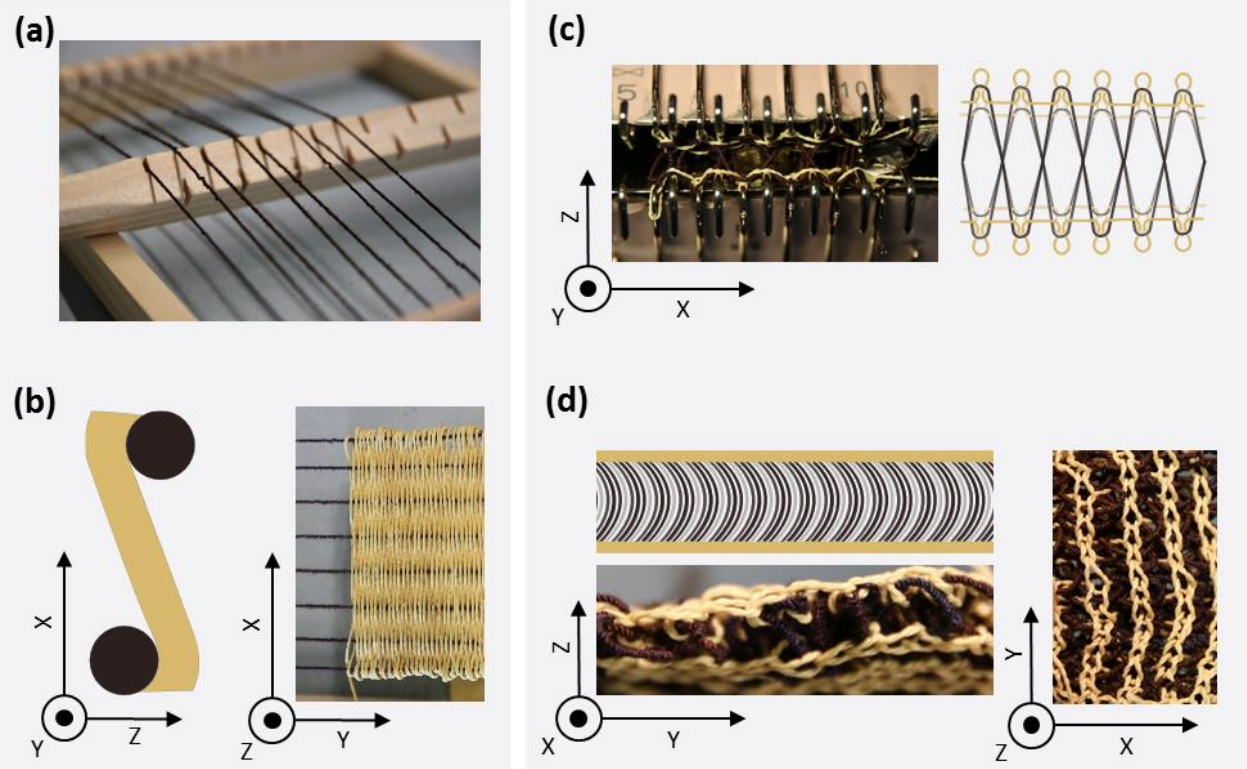

Figure 2. (a) NiTi coiled yarns stretched in the warp direction in the hobbyist loom with 8.5 mm spacing. (b) The Kevlar weft thread interweaving around the warp coiled yarns (left) and the coiled yarn woven in a mid- manufactured state (right). (c) Spacer fabric manufacturing on a Taitexma TH-860 (left), and a diagram of the spacer yarn pattern integrated across two Kevlar stockinette surfaces (right) (d) Finished spacer fabric depicted from the side view (left) and top view (right).

2.4 Experimental Methodology

Woven actuation testing was performed on a Instron 3365 equipped with an environmental chamber for controlling temperature. The woven textile was loaded on custom built fixtures to ensure loading was applied to the NiTi coiled yarns. Force block testing (iso-strain) was performed on the NiTi coiled yarn woven to understand the force generation for compression applications. To begin testing, the chamber is heated to 80ºC to heat the sample to austenite and remove any residual strains from handling. Slight manufacturing inconsistencies are mitigated by preloading the sample to 1 N to ensure all coiled yarn architectures are engaged. The length at this point is recorded as the austenite free length and is considered as the original length measurement for structural strain calculations. The sample is then cooled to -40ºC, below M_f, and soaked for five minutes before being displaced at a global rate of $\dot{\delta}L^{-1} = \pm 4 \times 10^{-4}\, s^{-1}$ to a set structural strain. The structural strain was fixed, and the sample was heated to 80ºC, soaked for five minutes. The same cooling and heating cycles were performed again before returning to -40ºC and increasing the displacement to the next set structural strain. Throughout testing, displacement and temperature are continuously controlled and force is being measured. Force generation, F_{gen}, is the key metric calculated from the results from force blocking testing and is defined as the difference between the martensitic force (F_{mar}) at the end of a cooling ramp, and the austenitic force (F_{aus}) at the end of the subsequent heating ramp (Equation 1);

$$F_{gen} = F_{aus} - F_{mar}. \quad (1)$$

For each structural strain hold, there are two force generations and the averages are used analytically. For compressional garment applications, a commonly used metric is unit tension, F_u, or the generated forces normalized by the width of the textile (Equation 2),

$$F_u = \frac{F_{gen}}{w}. \quad (2)$$

To better understand the performance of the woven actuator, isothermal displacement-controlled tests were performed on single coiled yarns on a TA Instruments RSA-G2 dynamic mechanical analyzer (DMA) equipped with an environmental chamber for controlling temperature. Testing was performed to extrapolate safe operating ranges, as well as estimates for effective austenitic and martensitic moduli. Force block testing was performed as well to investigate the generated force potential of a single coiled yarn in comparison with the woven actuator.

The energy absorption potential of the spacer fabric was investigated through slow, displacement controlled isothermal compression tests as well as dynamic testing performed on a TA Instruments RSA-G2 dynamic mechanical analyzer (DMA). Displacement controlled compression tests were performed at 80ºC, above A_f, at a global displacement rate of $\dot{\delta}L^{-1} = \pm 4 \times 10^{-4}\, s^{-1}$ with 25mm diameter compression plates corresponding to a testing area, A_{comp}, of $4.908x10^{-4}\, m^2$. Displacements and forces are converted to structural strain and pressure to quantify common spacer fabric and engineering metrics. In spacer fabric technologies, it's common to analyze the loading curve for the shape and amount of energy absorbed per unit volume (W), defined as the area under the pressure-strain loading curve. However, analysis of the unloading behavior is needed to understand the NiTi material impact within the spacer fabric structure. The dissipated energy per unit volume is defined as the area between the loading and unloading curve and offers insight into the forward and reverse martensitic transformations occurring in the NiTi coiled yarns during loading and unloading.

Lastly, dynamic mechanical testing was performed to isolate the vibration damping potential of NiTi coiled yarns. The damping performance of NiTi structures is known to be dependent on the prestrain, vibration amplitude, and vibration frequency [31]. Dynamic testing consisted of loading the NiTi coiled yarn sample to a fixed prestrain, before cycling through an oscillation strain with a corresponding amplitude and frequency. Oscillatory testing is used to quantify tan delta ($\tan\delta$), where delta (δ) is the phase lag between input strain and resulting stress. The tan delta, also known as the loss tangent, is commonly used as a key metric to analyzing damping performance. Tan delta is commonly used as an efficiency metric but does not offer much insight into the amount of energy that is being absorbed and dissipated, instead, the loss modulus, E'', represents the amount of energy absorbed and dissipated as heat.

3. FUNCTIONAL BEHAVIOR

3.1 Actuation Performance of Coiled Yarn Woven

The woven actuation performance was encouraging for artificial muscle application, specifically in a medical compression garment. The woven actuator could undergo large deformations, up to 55.0% structural strain, (Figure 3a). This is a significant increase on singled coiled yarns which typically fail in the 20% - 40% structural strain range and 8N (Figure 3d) and directly applies to the ability of the woven textile to be stretched over a large area of the body during donning. In single coiled yarns, the main mechanism of failure occurs when the axial tension pulls the NiTi microfilaments out of the coiled yarn architecture back into a yarn. The yarn section becomes the weakest point and fails with additional loading. There is a combination of reasons for the extended strain range of the woven textile compared with a single coiled yarn. First, the coiled yarns are in parallel, sharing the total applied load across each coiled yarn. It's assumed that due to manufacturing inconsistencies the load is not split evenly across each coiled yarn. It's theorized instead, the load is mainly applied to a single or couple coiled yarns. When those heavily loaded coiled yarns begin to weaken, either from stressed induced martensitic transformation or partial de-coiling, the load is transferred to a different, less loaded coiled yarn. This form of load sharing would allow the entire structure to be strained to large structural strains, beyond that of a single coiled yarn. It also explains why the woven is not exactly eight times stronger than a single coiled yarn. Additionally, it is theorized that the Kevlar weft yarn applies a compression on the coiled yarns, providing a resistant force against de-coiling.

During donning of a compression garment, it is desirable for the compression garment to provide the least amount of resistance as possible to make the experience easier on the user. For a SMA based compression garment, donning would occur in the less stiff martensitic phase and the woven actuator provides a low force response in the martensitic state (Figure 3a) [32]. At low structural strains (0-10.0%), an effective martensitic modulus can be estimated to be 29.84 MPa (Figure 3a). Compared with an effective austenitic modulus of 650.5 MPa, the NiTi coiled woven exhibits a 21.8 times change in effective stiffness between the two states, compared with a 2.46 times change in the single coiled yarn (Figure 3c).

Upon heating, the woven actuator generated large forces, up to 53.25N at 40.0% structural strain, which corresponds to a unit tension of $934.2\,\frac{N}{m}$ (Figure 3b). This aspect directly relates to generating pressures needed for there to be a medical benefit applied to the user. A promising aspect here is that the woven was not scaled for generated forces or optimized for

unit tension. To increase the generated forces, the original NiTi microfilament bundles could be adjusted to have more filaments, i.e. more active material or more coiled yarns could have been used. For unit tension, a loom with smaller spacings between warp yarns could be used, significantly reducing the amount of dead space between the active coiled yarn structures. Currently, the woven has a width of 57mm, with only 6.4mm consisting of active NiTi coiled yarn. The scalable, unoptimized NiTi coiled yarn woven actuator yields significant potential in medical compression applications due to large achievable structural strains, a near zero force martensitic response, large changes in modulus corresponding to large generated forces, and an innate wearability.

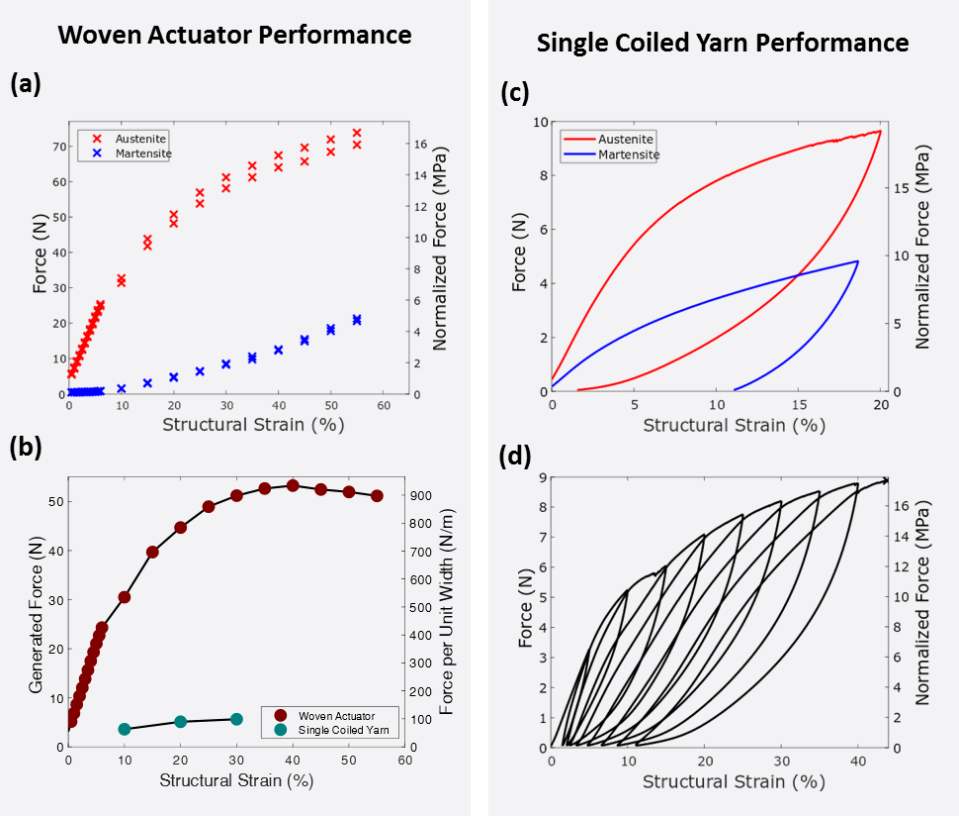

Figure 3. (a) The austenitic and martensitic force response during isostrain force block testing. The values can be used to estimate stiffness of the two states. A low martensitic force response and a large change in stiffness is observed between austenite and martensite, (b) Generated forces by the NiTi coiled yarn woven as well as the single coiled yarn during heating in the isostrain force block testing. The actuating woven was capable of generating forces up to 53.25N at 40.0% structural strain. (c) Isothermal pull-out curves for singled coiled NiTi yarn in austenite and martensite. These curves are used to compare with the woven actuator performance to isolate the impact of integrating with a textile structure. (d) Increased strain isothermal testing of a single coiled yarn to investigate the safe operating strains of the singled coiled yarn. The woven actuator exhibited the ability to undergo increased structural strains as a result of load sharing amongst the parallel coiled yarns.

3.2 Compression Behavior of Coiled Yarn Spacer Fabric

Typical compression behavior of a spacer fabric is split up in four distinct stages [33]-[34]. The first is a lower sloped linear region where the loose outer layers being engaged. This is followed by a higher linearly sloped region which corresponds to compression and light buckling of the spacer yarns. The third stage corresponds to a nearly constant stress plateau which is a result of additional buckling, rotating, and shearing of the spacer yarn. This is followed by a steep increase in stress from the densification of the fabric which restricts any further movement of the spacer yarn.

The NiTi coiled yarn spacer fabric did not exhibit typical spacer fabric compression behavior, however, it did still exhibit three distinct stages of compression behavior (Figure 4a). The first stage, I, (0% to 18.0% Structural Strain) corresponds to a light interaction of the fabric being engaged together demonstrated by a modulus estimation of 27 kPa. This is followed by a slightly stiffer linear region, II, (18.0% to 37.0%) with an estimated slope of 136 kPa, which is a combination of structural buckling, shearing, rotation of the coiled yarn as well as any stress induced martensitic transformation that may

be occurring. Like typical spacer fabric behavior, the last stage, III, is the densification of the spacer fabric where movement of the spacer yarns are prevented by interaction and a sharp increase in stress is exhibited. If any further detwinning occurred in the NiTi coiled yarns in this stage, it is being dominated by the densified state of the spacer fabric.

Analysis of the unloading behavior and comparison with the martensitic loading/unloading offers insight into the NiTi superelastic impact within the spacer fabric (Figure 4b). In austenite, the spacer fabric exhibited a large hysteresis between the loading and unloading curve, resulting in $6.67\frac{kJ}{m^3}$ of dissipated energy per unit volume. The energy dissipation is a combination of forward transformation within the NiTi material as well as friction within the coiled yarn and spacer fabric structures. To isolate the impact from forward transformation, compression loading in martensite was performed. During loading in martensite, NiTi undergoes an irreversible transformation from temperature induced martensite to stress induced martensite, upon unloading limited strain recoverability is observed. However, the spacer fabric martensitic curve still exhibited hysteresis corresponding to $3.99\frac{kJ}{m^3}$ of dissipated energy per unit volume. This signifies that structural friction shares a significant role dissipating energy along with traditional NiTi superelastic behavior. Additionally, the impact of superelastic NiTi can be observed in the strain recoverability of the spacer fabric in austenite compared with martensite. In austenite, the spacer fabric recovered 47.8% of the applied strain, compared with 40.0% in the martensitic curve (Figure 4b). While strain recoverability is dominated by structural effects (coiled yarn and fabric), superelastic behavior still plays a minor role.

The goal of integrating NiTi coiled yarns within a spacer fabric was to leverage both material and structural stress plateaus to improve spacer fabric performance. While the spacer fabric presented in this work is dominated more by structural effects, future iterations will seek to leverage more of the active material behavior by increasing the spacer fabric thickness, and altering the spacer yarn pattern to induce more buckling, shearing, and rotation of the spacer yarn. Leveraging both a material and structural stress plateau could improve spacer fabric energy absorbing performance.

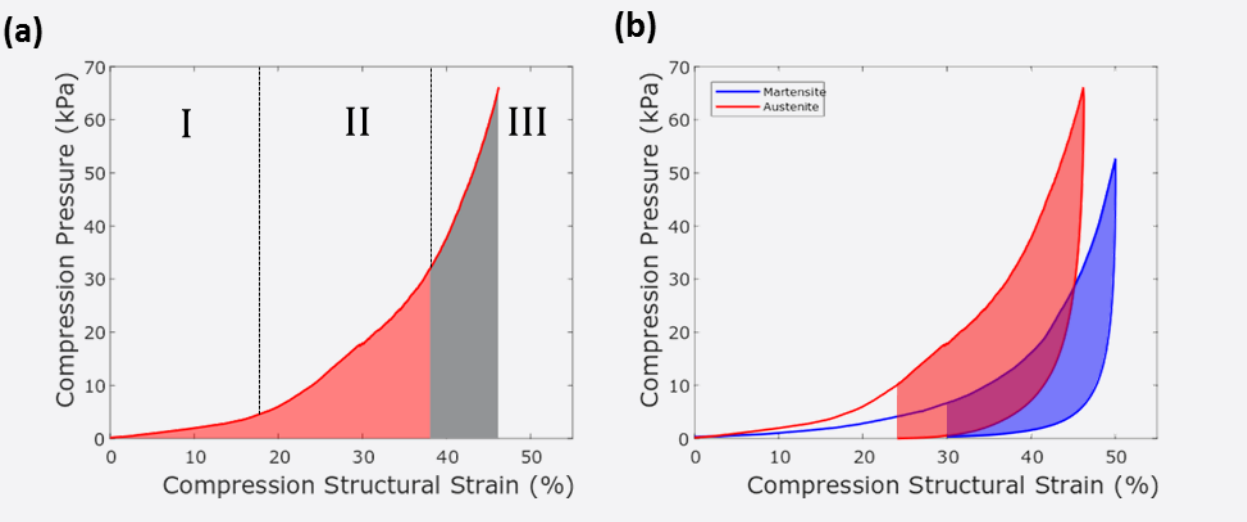

Figure 4. (a) Loading curve of the NiTi coiled yarn spacer fabric in austenite. The loading behavior is divided into three main stages: initial engagement, structural reorientation, and densification. (b) Loading and unloading of NiTi coiled yarn spacer fabric in austenite and martensite. These curves are used to isolate the material and structural dominated behavior in energy dissipation and strain recoverability.

3.3 Dynamic Behavior of Coiled Yarn Spacer Fabric

While quasi-static isothermal compression tests can give researchers a glimpse into the energy absorbing potential of a material or structure, dynamic oscillatory tests are more commonly used to characterize the damping performance. Six oscillatory tests with increasing oscillation frequencies and constant amplitudes are performed at five structural pre-strains to map the damping capability of the NiTi coiled yarn spacer fabric. It was found that the damping abilities were strongly correlated to the structural pre-strain applied to the spacer fabric (Figure 5). The tan delta, which offers insight into the ratio of elastic to viscous behavior in the sample, saw a slight increase at small pre-strains (0-20% structural prestrain) before tailing off at larger pre-strains (Figure 5a). In the superelastic SMA material system, viscous behavior can be

attributed to the forward and reverse martensitic transformation occurring. This means that when tan delta is a maximum, the sample may be undergoing its largest amount of stressed induced martensitic transformation, and austenitic recovery from the oscillating strain. Understanding how to maximum tan delta and the viscous response of the NiTi coiled yarn spacer fabric is essential to finding a coiled yarn and spacer structure that utilizes both structural and material effects to absorb and dampen mechanical energy. Additionally, the tan delta response of the fabric had a slight dependence on the oscillation frequency. Higher frequencies (10-40 Hz) corresponded to higher maximum tan deltas at smaller pre strains (10.0%) (Figure 5a). On the other hand, lower frequencies were able to maintain tan deltas near their maximums before tailing off at pre-strains greater than 20%. The lower frequencies allowed more time for the sample to undergo forward and reverse martensitic transformation, resulting in stable tan deltas over a larger pre-strain range.

To investigate the actual amount of energy dissipated by the SMA response, the loss modulus was calculated for each oscillatory test (Figure 5b). The loss modulus offers insight into the amount of energy being dissipated as heat. It was found that while the frequency had little to no impact on the loss modulus, the pre-strain had a large influence. Almost exactly mimicking the quasi-static compression test, the loss modulus is relatively small and linear at lower pre-strains before undergoing a steep increase during the densification of the spacer fabric. This makes sense as the loss modulus is scaled by the pressure exerted on the spacer fabric. However, even though the amount of energy being dissipated as heat is largest at 40% pre-strain, we know from the tan delta results that the ratio between the viscous and elastic behavior is at its lowest. This means that an even greater amount of energy is being stored linear elastically.

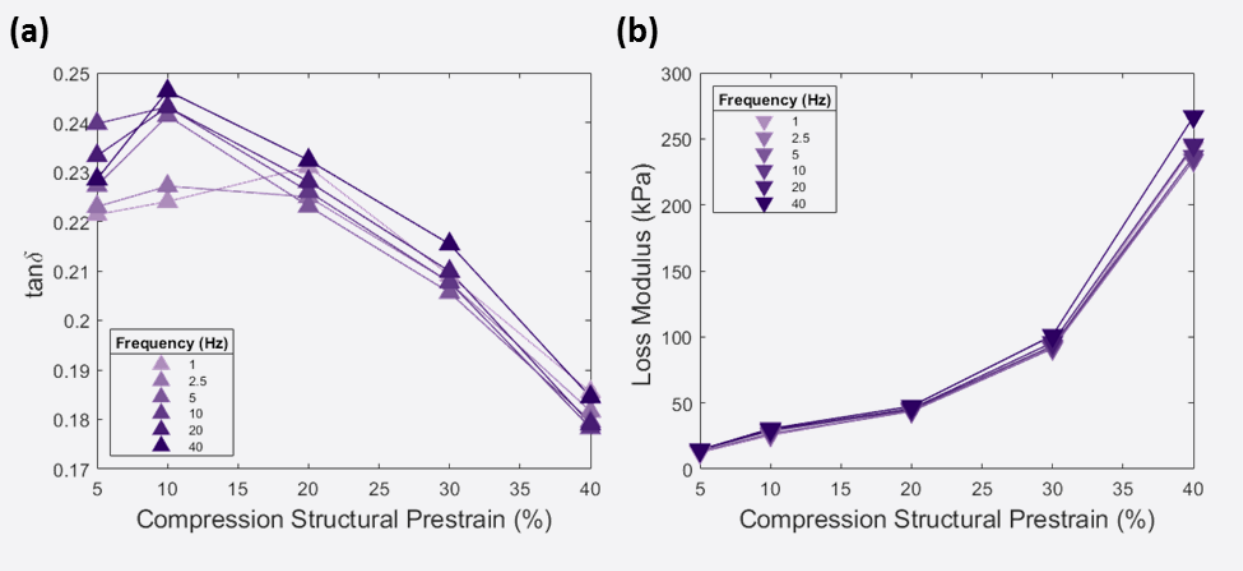

Figure 5.Dynamic oscillation test results on the NiTi coiled yarn spacer fabric to determine the relationship between oscillation frequency and structural prestrain on the tan delta (a) and loss modulus (b). These metrics signify the effectiveness of the damper to absorb and dissipate energy as well as the quantity of energy that is dissipated.

4. CONCLUSIONS

In this paper, we manufacture over-twisted NiTi coiled yarns and integrate their unique 1D structures into textiles for actuating and energy absorption applications. The coiled yarns are integrated in parallel in a woven actuating textile and characterized using force-block testing to quantify the generated force potential. The flexible, cloth-like woven actuator exhibits large, scalable generated forces at large structural strains from a solid-state phase transformation from martensite to austenite. A 21.8 times change in effective stiffness yields a martensite state with a low force response which is ideal for medical compression applications. Optimization and scaling of the woven actuator could provide significant unit tensions capable of producing pressures on the body to provide medicinal benefits to the user. Conversely, the 3D spacer fabric is manufactured with energy absorbing applications in mind such as impact absorption, and vibrational damping. Isothermal compression tests were performed to quantify energy absorption and understand coiled yarn spacer fabric kinematics. Dynamic oscillatory tests were performed to map relationships between pre-strain and frequency to loss

modulus and tan delta. Improvements for future iterations are discussed to better leverage superelastic material behavior as well as traditional textile effects. As first iteration textiles, NiTi coiled yarn integrated textiles offer a glimpse into the significant potential to offer tailored and improved actuations, vibrational damping, and energy absorption for a range of medical device, defense, transportation applications.

5. REFERENCES

[1] Di, J., Fang, S., Moura, F. A., Galvão, D. S., Bykova, J., Aliev, A., de Andrade, M. J., Lepró, X., Li, N., Haines, C., Ovalle-Robles, R., Qian, D. and Baughman, R. H., "Strong, Twist-Stable Carbon Nanotube Yarns and Muscles by Tension Annealing at Extreme Temperatures," Adv. Mater. **28**(31), 6598–6605 (2016).

[2] Persson, N.-K., Martinez, J. G., Zhong, Y., Maziz, A. and Jager, E. W. H., "Actuating Textiles: Next Generation of Smart Textiles," Adv. Mater. Technol. **3**(10), 1700397 (2018).

[3] Foroughi, J., Spinks, G. M., Wallace, G. G., Oh, J., Kozlov, M. E., Fang, S., Mirfakhrai, T., Madden, J. D. W., Shin, M. K., Kim, S. J. and Baughman, R. H., "Torsional Carbon Nanotube Artificial Muscles," Science **334**(6055), 494–497 (2011).

[4] Zhang, M., Atkinson, K., Baughman, R., "Multifunctional Carbon Nanotube Yarns by Downsizing an Ancient Technology," Science **306**(5700), 1358–1361 (2004).

[5] Smela, E., "Conjugated Polymer Actuators for Biomedical Applications," Advanced Materials **15**(6), 481–494 (2003).

[6] Carpi, F., Bauer, S. and Rossi, D. D., "Stretching Dielectric Elastomer Performance," Science **330**(6012), 1759–1761 (2010).

[7] Jeong, H.-K., Lee, J., Han, J.-H. and Wereley, N. M., "Design of frequency-tunable mesh washer isolators using shape memory alloy actuators," Journal of Intelligent Material Systems and Structures **27**(9), 1265–1280 (2016).

[8] Ula, S. W., Traugutt, N. A., Volpe, R. H., Patel, R. R., Yu, K. and Yakacki, C. M., "Liquid crystal elastomers: an introduction and review of emerging technologies," Liquid Crystals Reviews **6**(1), 78–107 (2018).

[9] Ware, T. H., McConney, M. E., Wie, J. J., Tondiglia, V. P. and White, T. J., "Voxelated liquid crystal elastomers," Science **347**(6225), 982–984 (2015).

[10] Naciri, J. W., Srinivasan, A. and Ratna, B. R., "Liquid crystal elastomer for artificial muscle applications," Smart Structures and Materials 2004: Electroactive Polymer Actuators and Devices (EAPAD) **5385**, 548–554, International Society for Optics and Photonics (2004).

[11] Shahsavan, H., Salili, S. M., Jákli, A. and Zhao, B., "Smart Muscle-Driven Self-Cleaning of Biomimetic Microstructures from Liquid Crystal Elastomers," Advanced Materials **27**(43), 6828–6833 (2015).

[12] Connolly, F., Polygerinos, P., Walsh, C. J. and Bertoldi, K., "Mechanical Programming of Soft Actuators by Varying Fiber Angle," Soft Robotics **2**(1), 26–32 (2015).

[13] Kothera, C. S., Jangid, M., Sirohi, J. and Wereley, N. M., "Experimental Characterization and Static Modeling of McKibben Actuators," J. Mech. Des **131**(9) (2009).

[14] Mirvakili, S. M. and Hunter, I. W., "Artificial Muscles: Mechanisms, Applications, and Challenges," Advanced Materials **30**(6), 1704407 (2018).

[15] Mu, J., de Andrade, M. J., Fang, S., Wang, X., Gao, E., Li, N., Kim, S. H., Wang, H., Hou, C., Zhang, Q., Zhu, M., Qian, D., Lu, H., Kongahage, D., Talebian, S., Foroughi, J., Spinks, G., Kim, H., Ware, T. H., et al., "Sheath-run artificial muscles," 7 (2019).

[16] Spinks, G. M., "Advanced Actuator Materials Powered by Biomimetic Helical Fiber Topologies," Advanced Materials **32**(18), 1904093 (2020).

[17] Park, J., Yoo, J. W., Seo, H. W., Lee, Y., Suhr, J., Moon, H., Koo, J. C., Choi, H. R., Hunt, R., Kim, K. J., Kim, S. H. and Nam, J.-D., "Electrically controllable twisted-coiled artificial muscle actuators using surface-modified polyester fibers," Smart Mater. Struct. **26**(3), 035048 (2017).

[18] Shang, Y., He, X., Li, Y., Zhang, L., Li, Z., Ji, C., Shi, E., Li, P., Zhu, K., Peng, Q., Wang, C., Zhang, X., Wang, R., Wei, J., Wang, K., Zhu, H., Wu, D. and Cao, A., "Super-Stretchable Spring-Like Carbon Nanotube Ropes," Adv. Mater. **24**(21), 2896–2900 (2012).

[19] Son, W., Chun, S., Lee, J. M., Lee, Y., Park, J., Suh, D., Lee, D. W., Jung, H., Kim, Y.-J., Kim, Y., Jeong, S. M., Lim, S. K. and Choi, C., "Highly twisted supercoils for superelastic multi-functional fibres," Nat Commun **10**(1), 426 (2019).

[20] Cherubini, A., Moretti, G., Vertechy, R. and Fontana, M., "Experimental characterization of thermally-activated artificial muscles based on coiled nylon fishing lines," AIP Advances **5**(6), 067158 (2015).

[21] Simeonov, A., Henderson, T., Lan, Z., Sundar, G., Factor, A., Zhang, J. and Yip, M., "Bundled Super-Coiled Polymer Artificial Muscles: Design, Characterization, and Modeling," IEEE Robotics and Automation Letters **3**(3), 1671–1678 (2018).

[22] Shaw, J., "Thermomechanical aspects of NiTi," Journal of the Mechanics and Physics of Solids **43**(8), 1243–1281 (1995).

[23] Nishida, M., Wayman, C. M. and Honma, T., "Precipitation processes in near-equiatomic TiNi shape memory alloys," Metallurgical Transactions A **17**(9), 1505–1515 (1986).

[24] Otsuka, K., Sawamura, T. and Shimizu, K., "Crystal structure and internal defects of equiatomic TiNi martensite," Phys. Stat. Sol. (a) **5**(2), 457–470 (1971).

[25] Eckelmeyer, K. H., "THE EFFECT OF ALLOYING ON THE SHAPE ~24DRY PHENOMENON IN NITINOL," 6.

[26] Todoroki, T. and Tamura, H., "Effect of Heat Treatment after Cold Working on the Phase Transformation in TiNi Alloy," Trans. JIM **28**(2), 83–94 (1987).

[27] Favier, D., Liu, Y., Orgéas, L., Sandel, A., Debove, L. and Comte-Gaz, P., "Influence of thermomechanical processing on the superelastic properties of a Ni-rich Nitinol shape memory alloy," Materials Science and Engineering: A **429**(1), 130–136 (2006).

[28] Pelton, A. R., Russell, S. M. and DiCello, J., "The physical metallurgy of nitinol for medical applications," JOM **55**(5), 33–37 (2003).

[29] Shaw, J. A., Churchill, C. B. and Iadicola, M. A., "TIPS AND TRICKS FOR CHARACTERIZING SHAPE MEMORY ALLOY WIRE: PART 1-DIFFERENTIAL SCANNING CALORIMETRY AND BASIC PHENOMENA," Experimental Techniques **32**(5), 55–62 (2008).

[30] Chen, X., [Advances in 3D Textiles], Elsevier (2015).

[31] Heller, L., Vokoun, D., Šittner, P. and Finckh, H., "3D flexible NiTi-braided elastomer composites for smart structure applications," Smart Mater. Struct. **21**(4), 045016 (2012).

[32] Eschen, K., Granberry, R., Holschuh, B. and Abel, J., "Amplifying and Leveraging Generated Force Upon Heating and Cooling in SMA Knitted Actuators," ACS Appl. Mater. Interfaces **12**(48), 54155–54167 (2020).

[33] Liu, Y., Hu, H., Zhao, L. and Long, H., "Compression behavior of warp-knitted spacer fabrics for cushioning applications," Textile Research Journal **82**(1), 11–20 (2012).

[34] Hamedi, M., Salimi, P. and Jamshidi, N., "Improving cushioning properties of a 3D weft knitted spacer fabric in a novel design with NiTi monofilaments," Journal of Industrial Textiles **49**(10), 1389–1410 (2020).